Supporting Information Appendix

Structure and mechanotransmission mechanism of the MacB ABC transporter superfamily

Allister Crow, Nicholas P. Greene*, Elise Kaplan, Vassilis Koronakis*

**Joint first authorship*

Supplemental Figures

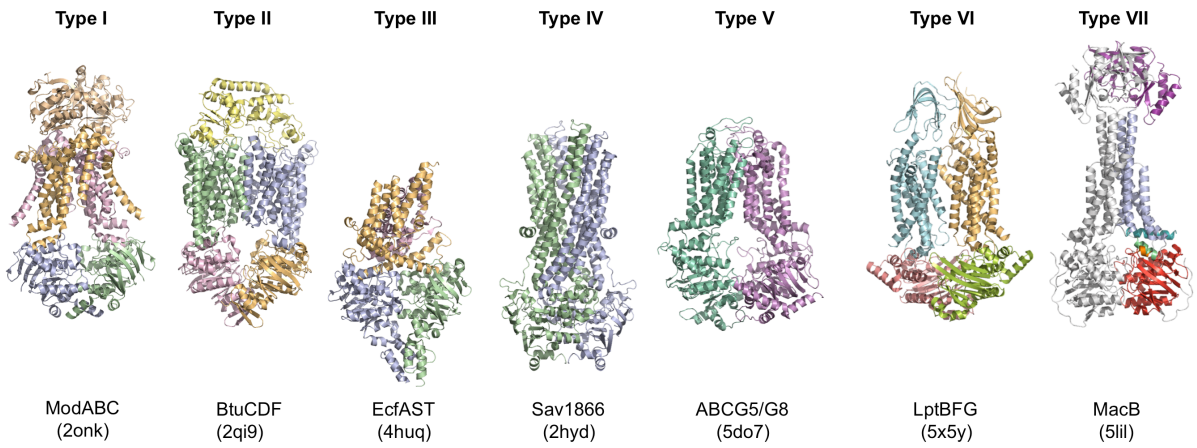

Figure S1: Seven ABC transporter superfamilies. ABC transporters of known structure fall into seven distinct superfamilies that are readily discerned by their 3-dimensional fold. An example from each superfamily is presented. From left to right the molybdate transporter (1) (ModABC), vitamin B_{12} transporter (2) (BtuCDF), folate importer (3) (EcfAST), multidrug exporter (4) (Sav1866), the sterol transporter (5) (ABCG5/G8), LPS extractor (6) (LptBFG) and the enterotoxin and macrolide transporter (MacB). Folds are named by extension of a previously established convention (7). PDB codes are shown in parentheses.

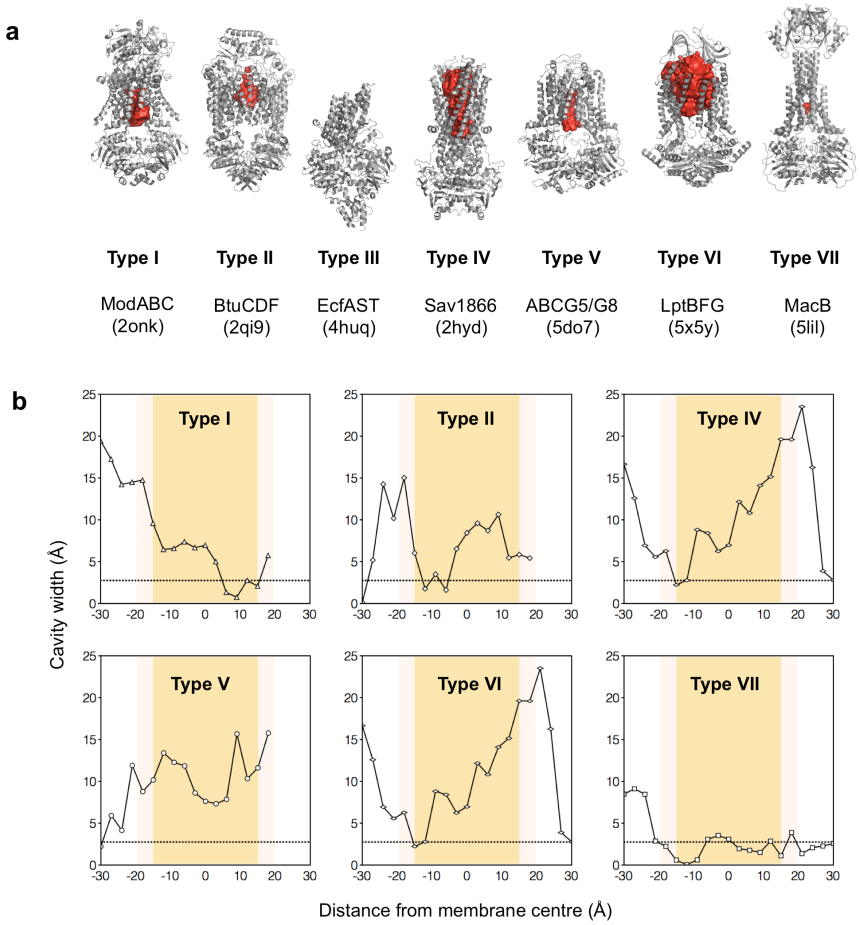

Figure S2: Intramembrane cavity analysis for ABC transporter superfamilies. (a) Visualisation of central transmembrane cavities as solid red 'casts' produced using HOLLOW (8). Sav1866 (4) and BtuCDF (2) are in outward-facing conformations, ModABC (1) and ABCG5/G8 (5) are both inward facing. MacB does not possess any significant cavities in either the transmembrane domain or periplasmic stalk. (b) Plots of cavity diameter at 3 Å intervals across the membrane region, from cytoplasm (-30 Å) to periplasm (+30 Å), are shown for MacB and five other ABC transporters. The 30 Å hydrophobic membrane core is shaded orange (-15 Å to +15 Å) with the lipid head group region in a lighter tone. The horizontal line represents the diameter of a water molecule (2.75 Å), only the region above the horizontal dotted line is solvent accessible. Analysis used the PoreWalker server (9).

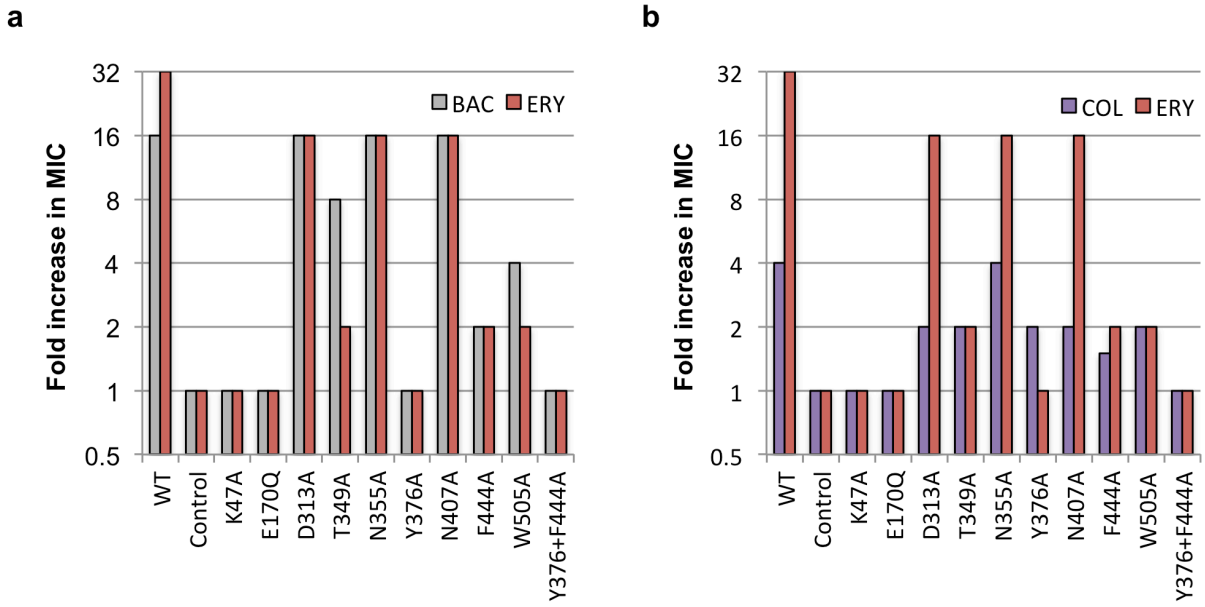

Figure S3: MacB periplasmic domain variants impaired in erythromycin tolerance have similar impairments in bacitracin and colistin resistance. (a) Comparison of bacitracin MIC data with erythromycin. (b) Comparison of colistin MIC data with erythromycin. Coloured bars represent fold increase in median MIC using the E170Q variant as the reference. Full details of the MIC data are provided in **Table S5**.

Figure S4

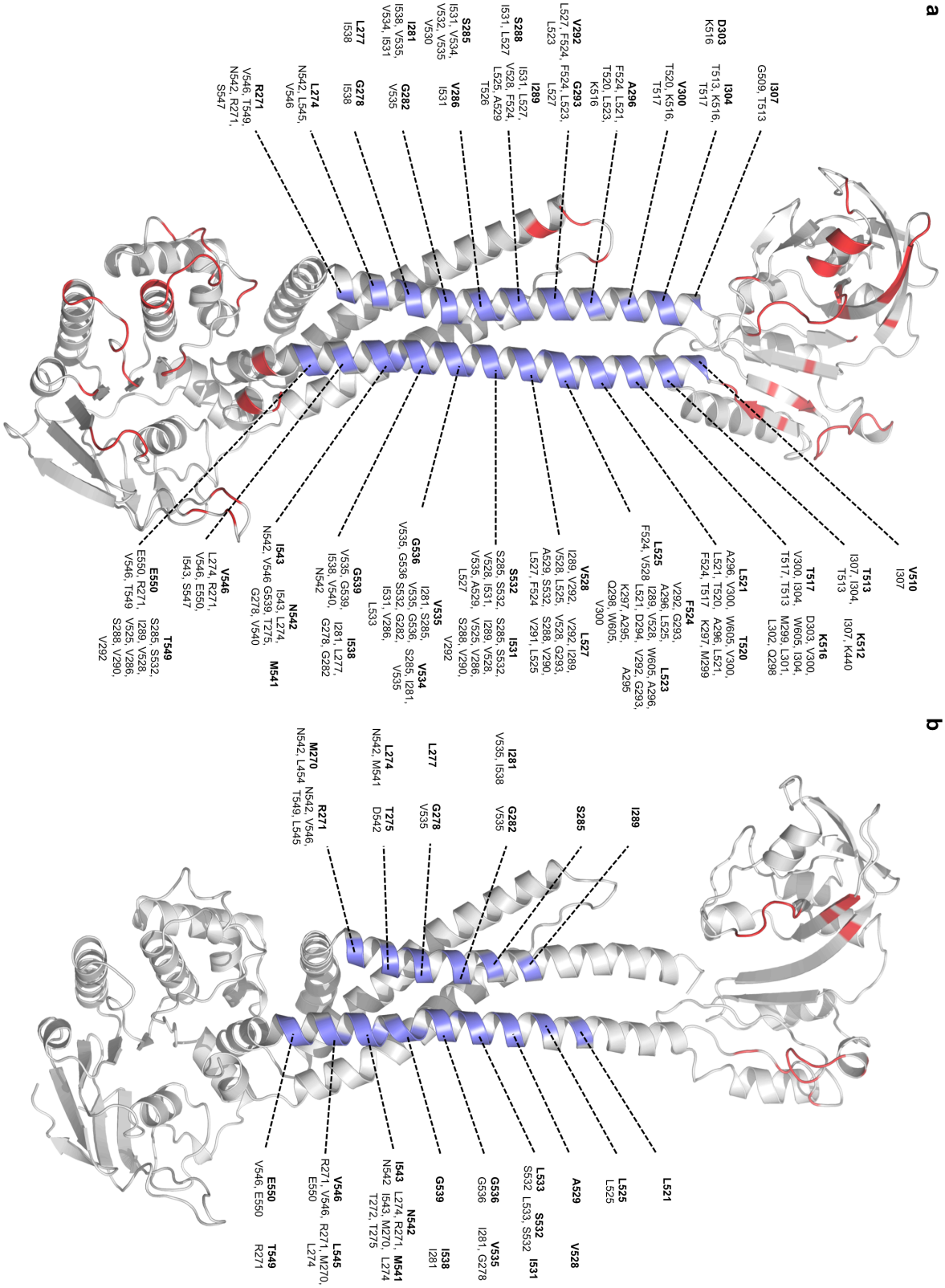
a
V510
I307
T513
I307, I304,
T513
K512
I307, K440
K516
D303, V300,
W605, I304,
M299, L301,
L302, Q298
T517
V300, I304,
T517, T513
L521
A296, V300, W605, V300,
L521, T520, A296, L521,
F524, T517, K297, M299
T520
F524
V292, Q293,
A296, L525,
I289, V528, W605, A296,
F524, V528 L521, D294, V292, Q293,
K297, A295, A295
Q298, W605,
V300
L523
V528
I289, V292,
V528, L525,
A529, S532,
L527, F524
V292, I289,
V528, Q293,
S288, V290,
V291, L525
L527
S532
S285, S532,
V528, I531,
V535, A529,
L527
S285, S532,
I289, V528,
V525, V286,
S288, V290,
V292
I531
V535
I281, S285,
V535, G536,
S532, G282,
I531, V286,
L533
G536
V534
I281, G278,
V535, G539,
I538, V540,
N542
V535, G539,
I538, V540,
G278, G282
I538
I281, L277,
G278, G282
N542
I543, L274,
N542, V546 G539, T275,
G278, V540
M541
I543
V546
L274, R271,
V546, E550,
I543, S547
E550
R271,
V546, T549
S285, S532,
I289, V528,
V525, V286,
S288, V290,
V292
T549
L277
I538
G278
I538
L274
N542, L545,
V546
R271
V546, T549,
N542, R271,
S547
I307
G509, T513
I304
T513, K516,
T517
V300
T520, K516,
T517
A296
F524, L521,
T520, L523,
K516
G293
L527, F524, L523,
L523
V292
L527, F524,
L523
I289
L527,
S288
I531, L527
V528, F524,
L525, A529,
T526
V286
I531
S285
I531, V534,
V532, V535
V530
I281
I538, V535,
V534, I531
G282
V535
b
I289
S285
G282
V535
I281
V535, I538
L277
G278
V535
L274
N542, M541
T275
D542
R271
N542, V546,
T549, L545
M270
N542, L454
L521
L525
L525
A529
S532, S533
L533
V528
S532
I531
G536
I281, G278
G536
V535
G539
I538
I281
I543
N542
N542
L274, R271,
I543, M270,
T272, T275
M541
L274
V546
R271, V546,
E550
L545
R271, M270,
L274
E550
V546, E550
T549
R271

Figure S4: Dimer interfaces for ATP-bound and nucleotide-free MacB. (a) Face-on view of the interface for a monomer of an *E. coli* MacB homology model based on the ATP-bound *A. actinomycetemcomitans* MacB structure. (b) Equivalent view of a monomer from *E. coli* MacB extracted from the cryoEM structure of the MacAB-TolC assembly (5NIL). Residues at the interface were identified with PISA (10) and contact sites defined using a 5 Å cut-off. Contact residues belonging to either TM1 or TM2 are coloured blue, and contacts elsewhere are coloured red. Residues belonging to TM1 or TM2 are annotated in bold with residues they contact across the dimer interface noted beneath in plain font. For clarity, residues falling on the same 'rung' of a helix are noted side-by-side with a single marker drawn to locate that rung on the structure.

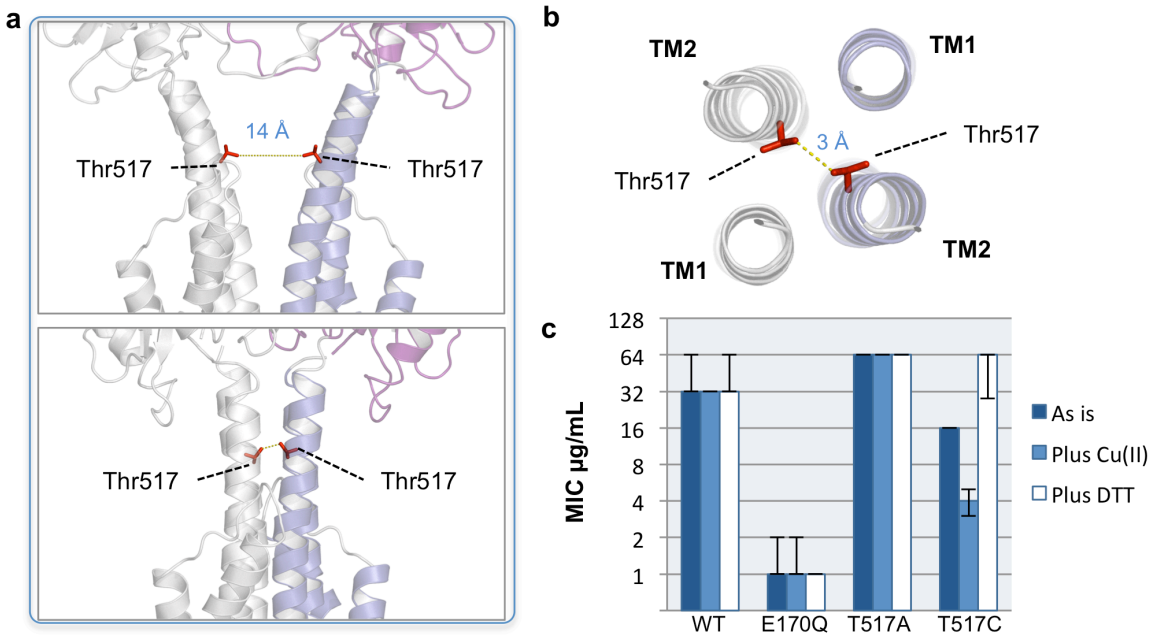

Figure S5: Locking the MacB periplasmic stalk using cysteine disulfide cross-links. (a) Location of Thr517 in nucleotide-free (*top*) and ATP-bound MacB (*bottom*). (b) Top-down view of the stalk showing position of Thr517 in the dimer interface. (c) MacB activity assessed using erythromycin MIC data. Coloured bars represent median values with the interquartile range shown as a black line.

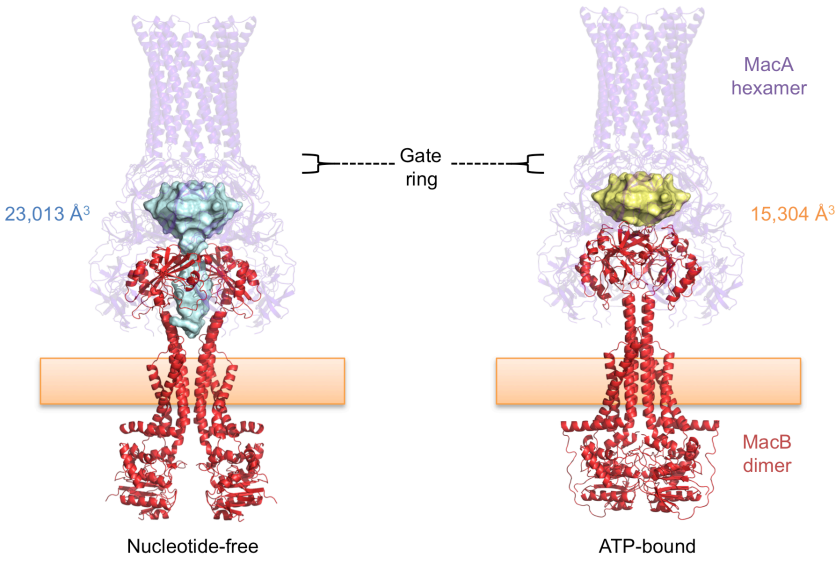

Figure S6: Volumetric analysis of the MacAB-TolC assembly. A central cavity at the interface between MacA and MacB undergoes a significant decrease in volume upon closure of the MacB periplasmic domains during ATP-binding. Models of the assembly in nucleotide-free and ATP-bound forms are shown on the *left* and *right*, respectively. Cavities are shown as solid casts with colour-coded volumes indicated alongside. TolC is omitted for clarity.

Supplemental Tables

Table S1: Crystallographic data and refinement statistics for soluble domain structures of *E. coli* MacB

	Periplasmic domain	Cytoplasmic NBD (form I)	Cytoplasmic NBD (form II)
PDB code	5LJ8	5LJ9	5LJA
Data collection			
Beam line	DLS I24	DLS I24	DLS I24
Wavelength (Å)	0.96861	0.96861	0.96862
Crystal parameters			
Space group	$P2_1$	$P6_122$	$C222_1$
Unit cell dimensions (Å)	50.1, 54.9, 66.9	56.0, 56.0, 259.1	57.5, 96.2, 262.7
Unit cell angles (°)	90, 92.9, 90	90, 90, 120	90, 90, 90
Mosaic spread (°)	0.68	0.43	0.50
Reflection data *			
Resolution range (Å)	32.87-1.95 (2.00-1.95)	48.48-2.40 (2.49-2.40)	52.54-2.30 (2.38-2.30)
Unique reflections	26,585 (1,874)	10,332 (1,044)	31,381 (2,615)
R_{sym}	0.089 (0.542)	0.096 (0.820)	0.077 (0.431)
I/σ(I)	8.1 (1.9)	12.2 (1.8)	14.0 (4.9)
$CC_{½}$	0.99 (0.70)	1.00 (0.69)	0.998 (0.92)
Completeness (%)	99.8 (99.7)	100.0 (100.0)	95.2 (82.4)
Multiplicity	3.4 (3.2)	7.6 (4.9)	6.6 (6.3)
Wilson B ($Å^2$)	21.5	39.8	31.8
Refinement †			
Resolution (Å)	66.8 – 1.95	48.48 – 2.40	52.54-2.30
Number of reflections	25,260	9,759	29,723
R_{work}	0.178	0.223	0.186
R_{free}	0.228	0.297	0.225
Rms (bond lengths) (Å)	0.017	0.013	0.016
Rms (bond angles) (°)	1.66	1.73	1.73
Model composition			
Protein atoms	3,266	1,801	5,450
Waters	99	9	199
Model B-factors			
Protein atoms ($Å^2$)	25.8	56.1	39.4
Waters ($Å^2$)	29.4	48.9	36.6
Ramachandran statistics ‡			
Favoured (%)	99.0	97.4	97.9
Allowed (%)	0.8	2.6	2.1
Outliers (%)	0.3	0.0	0.0

* As reported by Aimless (19).
† As reported by Refmac (26).
‡ As reported by Rampage (28).
Values in parentheses indicate the outer resolution bin.

Table S2: Crystallographic data and refinement statistics for *A. actinomycetemcomitans* MacB

	Seleno-MacB Hexagonal	MacB Hexagonal	MacB Monoclinic I	MacB Monoclinic II
PDB code	-	5LJ6	5LIL	5LJ7
Data collection				
Beam line	DLS I24	DLS I24	Soleil PX2	DLS I24
Wavelength (Å)	0.91732	0.97943	0.9763	0.96861
Crystal parameters				
Space group	$P6_522$	$P6_522$	$P2_1$	$P2_1$
Unit cell dimensions (Å)	119.01, 119.01, 300.87	119.57, 199.57, 307.78	111.59, 82.62, 124.92	112.33, 82.61, 125.17
Unit cell angles (°)	90, 90, 120	90, 90, 120	90, 94.45, 90	90, 93.54, 90
Mosaic spread (°)	0.63	0.80	0.98	0.71
Number of crystals	1	1	3	1
Reflection data *				
Resolution range (Å)	60.17-5.00 [60.17-11.18] (5.59-5.00)	61.56-3.90 [61.56-8.72] (4.36-3.90)	79.95-3.35 [79.95-10.59] (3.53-3.35)	86.13-3.25 [86.13-11.26] (3.39-3.25)
Unique reflections	5,997 [635] (1,624)	12,392 [1,297] (3,286)	32,862 [1,110] (4,631)	36,201 [901] (4,429)
R_{sym}	0.145 [0.052] (1.792)	0.103 [0.051] (2.466)	0.284 [0.064] (1.522)	0.210 [0.071] (1.317)
R_{meas}	0.152 [0.057] (1.842)	0.108 [0.053] (2.585)	0.301 [0.069] (1.617)	0.230 [0.078] (1.436)
R_{pim}	0.028 [0.011] (0.324)	0.029 [0.015] (0.651)	0.099 [0.026] (0.541)	0.092 [0.033] (0.565)
I/σ(I)	16.1 [49.7] (3.1)	10.3 [36.5] (1.8)	7.7 [28.4] (2.1)	6.7 [17.6] (1.7)
CC½	1.00 (0.388)	0.997 (0.652)	0.993 (0.790)	0.995 (0.799)
Completeness (%)	100.0 [99.5] (100.0)	97.9 [99.8] (94.8)	99.6 [99.8] (97.1)	99.4 [96.6] (99.9)
Multiplicity	31.3 [26.2] (32.2)	13.8 (13.0)	9.3 (8.9)	6.1 (6.2)
Wilson B ($Å^2$)	291	215	125	38
Refinement †				
Resolution (Å)	-	59.79-3.90	79.95-3.35	86.13-3.25
Reflections	-	12,315	32,620	36,080
R_{work}	-	0.2675	0.2444	0.2447
R_{free}	-	0.3222	0.2902	0.2994
Rms (bond lengths) (Å)	-	0.004	0.003	0.003
Rms (bond angles) (°)	-	1.025	0.711	0.637
Model composition				
MacB	-	1	2	2
ATP	-	1	2	2
Mg^{2+}		1	2	2
Waters	-	-	4	4
Model B-factors				
MacB ($Å^2$)	-	239	100	103
ATP/Mg^{2+} ($Å^2$)	-	225	70	75
Waters ($Å^2$)	-	159	56	55
Ramachandran statistics ‡				
Favoured (%)	-	91.69	93.84	93.14
Allowed (%)	-	7.63	5.75	6.60
Outliers (%)	-	0.68	0.42	0.26

* As reported by Aimless (19).
† As reported by Refmac (26).
‡ As reported by Rampage (28).
Values in parentheses indicate the outer resolution bin.
Values in square brackets indicate the inner resolution bin..

Table S3: Antimicrobial susceptibility testing. MIC expressed as µg/mL.

Antimicrobial	Num. repeats		Mean±SD MIC		Median±SIQR MIC	
	WT	E170Q	WT	E170Q	WT	E170Q
Erythromycin (ERY)	24	24	31±3	1±0	32±8	1±0
Bacitracin (BAC)	24	24	8021±836	490±72	8192±0	512±0
Colistin (COL)	32	32	23±8	4±1	16±4	4±0
Kanamycin (KAN)	8	8	32±0	18±6	32±0	16±0
Chloramphenicol (CHL)	8	8	1±1	1±1	1±1	1±0
Ciprofloxacin (CIP)	8	8	1±0	1±0	1±0	1±0
Tetracycline (TET)	8	8	2±0	2±0	2±0	2±0
Gentamycin (GEN)	3	3	15±2	16±0	16±0	16±0
Sodium dodecyl sulphate (SDS)	8	8	>256	>256	>256	>256
Chlorhexidine (CHX)	8	8	2±0	2±1	2±1	2±0
Ethidium bromide (EBR)	8	8	2±0	2±0	2±0	2±0

Minimum Inhibitory Concentrations (MICs) expressed as µg/mL.

Mean±SD corresponds to the arithmetic mean ± standard deviation.

Median±SIQR corresponds to the median value ± semi-interquartile range.

Table S4: Erythromycin MIC data for wild type and variant MacB

Variant	Repeats	Mean±SD MIC	Median±SIQR MIC	Location	STII export
WT	32	40±15	32±4	-	+
Control	32	1±1	1±0.5	-	-
K47A	24	1±1	1±0.5	NBD	-
R121A	24	7±2	8±2	NBD	+
E170Q	24	1±0	1±0	NBD	-
E256A	24	24±14	16±8	Amphipathic helix	+
T275A	24	8±0	8±0	TM1	+
S285A	24	22±8	16±8	TM1	+
T311A	24	29±11	32±8	Porter I	+
D313A	24	21±8	16±8	Porter I	+
Y315A	24	6±2	4±2	Porter I	+
K318A	24	14±5	16±4	Porter I	+
D319A	24	7±3	8±2	Porter I	+
F320A	24	3±1	4±1	Porter I	+
D322A	24	13±4	16±4	Porter I	+
D323A	24	11±4	8±4	Porter I	+
D324A	24	19±10	16±12	Porter I	+
Q326A	24	32±0	32±0	Porter I	+
Y327A	24	16±8	16±4	Porter I	+
Q328A	24	32±0	32±0	Porter I	+
Q329A	24	28±7	32±2	Porter I	+
N335A	24	33±7	32±0	Porter I	+
T349A	24	2±1	2±0	Porter I	+
S353A	24	22±8	16±8	Sabre	+
N355A	24	21±8	16±8	Sabre	+
R357A	24	11±4	8±4	Sabre	+
R359A	24	13±4	16±4	Sabre	+
N361A	24	27±7	32±8	Sabre	+
N362A	24	28±11	32±8	Sabre	+
D364A	24	22±8	16±8	Sabre	+
S368A	24	14±4	16±1	Sabre	+
N370A	24	27±8	32±8	Sabre	+
V372A	24	15±6	16±1	Sabre	+
Y376A	24	1±0	1±0	Sabre	+
D405A	24	21±8	16±8	Sabre	+
S406A	24	27±8	32±8	Sabre	+
N407A	24	13±4	16±4	Sabre	+
R409A	24	27±8	32±8	Sabre	+
R410A	24	14±4	16±4	Sabre	+
Q411A	24	43±22	48±24	Sabre	+
N428E	24	84±32	64±32	Sabre	+
E438A	24	43±15	32±16	Sabre	+
E439A	24	41±17	32±16	Sabre	+

K440A	24	8±6	8±2	Sabre	+
Q441A	24	27±8	32±8	Sabre	+
S442A	24	9±3	8±0	Sabre	+
M443A	24	7±3	8±2	Sabre	+
F444A	24	2±1	2±0.5	Sabre	+
S446A	24	21±7	16±8	Sabre	+
S447A	24	8±2	8±0	Sabre	+
K448A	24	32±0	32±0	Sabre	+
R451A	24	9±3	8±0	Sabre	+
W453A	24	32±16	32±8	Sabre	+
Y456A	24	26±8	32±8	Sabre	+
R462E	24	43±15	32±16	Sabre	+
S471A	24	11±4	8±4	Porter II	+
T473A	24	21±8	16±8	Porter II	+
E486A	24	7±6	4±2	Porter II	+
H497A	24	32±23	32±8	Porter II	+
K499A	24	27±8	32±8	Porter II	+
K500A	24	52±16	64±16	Porter II	+
D501A	24	21±8	16±8	Porter II	+
F503A	24	4±1	4±0	Porter II	+
W505A	24	2±1	2±0	Porter II	+
M507A	24	3±1	3±1	Porter II	+
T517A	24	87±33	64±32	Stalk	+
T520A	24	64±46	32±48	Stalk	+
S532A	24	30±15	32±8	TM2	+
N542A	24	32±0	32±0	TM2	+
D322A+D323A+D324A	24	4±1	4±0	Porter	+
Y376A+F444A	24	1±0	1±0	Sabre	+
E438A+E439A	24	43±15	32±16	Sabre	+
Δ C-terminus	24	8±4	8±2	Minor coupling helix	+

Minimum Inhibitory Concentrations (MICs) expressed as μg/mL.

Mean±SD corresponds to the arithmetic mean ± standard deviation.

Median±SIQR corresponds to the median value ± semi-interquartile range.

The MacB periplasmic domain is made up of both Porter and Sabre subdomains. The Porter itself is formed from two discontinuous regions of primary sequence labelled here as Porter I and Porter II.

Abbreviations used: NBD, Nucleotide binding domain; TM1 and TM2, transmembrane helix 1 and transmembrane helix 2.

Table S5: Bacitracin and Colistin MIC data for MacB variants.

	Bacitracin			Colistin			
Variant	**N**	**Mean±SD**	**Median±SIQR**	**N**	**Mean±SD**	**Median±SIQR**	**Location**
WT	24	4096±0	4096±0	24	16±0	16±0	-
Control	24	277±72	256±0	24	6±2	4±2	-
K47A	24	256±0	256±0	24	6±2	4±2	NBD
E170Q	24	251±26	256±0	24	5±2	4±2	NBD
D313A	24	4096±0	4096±0	24	8±2	8±0	Porter I
T349A	24	2048±0	2048±0	24	10±5	8±6	Porter I
N355A	24	4096±0	4096±0	24	18±11	16±12	Sabre
Y376A	24	331±118	256±0	24	6±2	8±2	Sabre
N407A	24	3413±986	4096±1024	24	11±4	8±4	Sabre
F444A	24	491±72	512±0	24	6±2	6±2	Sabre
W505A	24	1024±0	1024±0	24	7±2	8±2	Porter II
Y376A+ F444A	24	352±127	256±128	24	5±2	4±2	Sabre

Minimum Inhibitory Concentrations (MICs) expressed as µg/mL.

N = number of repeats.

Mean±SD corresponds to the arithmetic mean ± standard deviation.

Median±SIQR corresponds to the median value ± semi-interquartile range.

Table S6: Cysteine-locking experiment MIC data.

	-			+ $Cu(II)Cl_2$			+DTT		
Variant	**N**	**Mean ±SD**	**Median ±SIQR**	**N**	**Mean ±SD**	**Median ±SIQR**	**N**	**Mean ±SD**	**Median ±SIQR**
WT	24	43±15	32±16	24	32±0	32±0	24	43±15	32±16
E170Q	24	1±1	1±1	24	2±1	1±1	24	1±0	1±0
T517A	16	64±0	64±0	16	62±8	64±0	16	64±0	64±0
T517C	16	16±0	16±0	16	5±2	4±1	16	46±21	64±18

Minimum Inhibitory Concentrations (MICs) for erythromycin expressed as µg/mL.

N = number of repeats.

Mean±SD corresponds to the arithmetic mean ± standard deviation.

Median±SIQR corresponds to the median value ± semi-interquartile range.

Table S7: Crystallographic data and refinement statistics for the periplasmic domain of *E. coli* LolC

	Periplasmic domain of *E. coli* LolC
PDB code	5NAA
Data collection	
Beam line	I03
Wavelength (Å)	0.9763
Crystal parameters	
Space group	C2
Unit cell dimensions (Å)	54.7, 111.8, 75.9
Unit cell angles (°)	90, 109, 90
Mosaic spread (°)	0.84
Reflection data *	
Resolution range (Å)	45.99-1.88 (1.92-1.88)
Unique reflections	34,822 (2,179)
R_{sym}	0.078 (0.436)
I/σ(I)	11.0 (2.4)
CC½	0.996 (0.759)
Completeness (%)	99.5 (98.1)
Multiplicity	5.1 (3.9)
Wilson B ($Å^2$)	24.8
Refinement †	
Resolution (Å)	45.99 (1.88)
Number of reflections	32,931
R_{work}	0.1798
R_{free}	0.2252
Rms (bond lengths) (Å)	0.018
Rms (bond angles) (°)	1.81
Model composition	
Protein atoms	3,467
Waters	240
Other	5
Model B-factors	
Protein atoms ($Å^2$)	32.9
Waters ($Å^2$)	37.0
Other	60.2
Ramachandran statistics ‡	
Favoured (%)	98.4
Allowed (%)	1.6
Outliers (%)	0.0

* As reported by Aimless(19).
† As reported by Refmac (26).
‡ As reported by Rampage (28).
Values in parentheses indicate the outer resolution bin.

Supplementary Methods

Construction of strains and plasmids

pET28-EcMacB, encoding N-terminally His-tagged *E. coli* MacB, was created by PCR amplification of *macB* from *E. coli* MG1655 genomic DNA, digestion with NdeI and BamHI, and ligation into pET28 (Novagen) digested with the same enzymes. MacB homologues from *A. actinomycetemcomitans, A. pleuropneumoniae, P. aeruginosa, P. syringae, R. capsulatus, S. marcescens, S. typhimurium* and *P. mirabilis* were cloned with a similar strategy. *A. actinomycetemcomitans* E169Q and *E. coli* E170Q MacB mutants were introduced by Quikchange site-directed mutagenesis. Plasmids expressing the *E. coli* MacB NBD (pMacB-NBD; residues 1-223) and the periplasmic domain (pMacB-Peri; residues 309-508) with C-terminal His-tags were created by PCR amplification of *E. coli* MG1655 genomic DNA, digestion of PCR products with NdeI and XhoI, and ligation into pET21a digested with the same enzymes. *E. coli macA* was cloned NdeI-XhoI into the second multiple cloning site (MCS) of pETDuet1 (Novagen) resulting in pDuet-MacA. For co-expression of *E. coli* MacAB, wild type *macB* was cloned NcoI-HindIII into the first MCS of pET-MacA resulting in pETDuet-MacAB. Point mutants were introduced into pETDuet-MacAB by Quikchange site-directed mutagenesis. Heat stable enterotoxin was amplified from pET11-STII (11) and cloned into pCDFDuet using NcoI and KpnI restriction sites resulting in pCDF-STII. The *E. coli* LolC periplasmic domain predicted by Octopus (12) (residues 48-266) was amplified from *E. coli* MG1655 genomic DNA, digested with NdeI and NotI and ligated into pET24 digested with the same enzymes resulting in pET24-EcperLolC. All clones were verified by DNA sequencing (Source Bioscience). The *macAB* locus in *E. coli* C43 (DE3) (13) was replaced with a kanamycin resistance cassette using the λ Red recombinase system (14). The resistance cassette was subsequently removed by transformation with plasmid pCP20 encoding the FLP recombinase (15) resulting in strain C43 (DE3) Δ*macAB*. Strain C43 (DE3) Δ*acrAB* Δ*macAB* was created by subsequent removal of *acrAB* in the same manner. Both deletions were confirmed by PCR of the gene locus.

Enterotoxin secretion assay

C43 (DE3) or C43 (DE3) Δ*macAB* bearing pCDF-STII and plasmid-borne *mac* genes as indicated were grown in 2YT medium at 37 °C until an OD_{600} of 0.4 was achieved. Protein production was induced with 0.5 mM IPTG and cultures grown for a further 2 hours. Cells were removed by centrifugation at 4000 *g* and the supernatant passed through a 0.22 μm filter. Supernatant samples (1 mL) were precipitated with 10 % trichloroacetic acid (final concentration), washed with acetone and then resuspended in SDS-PAGE loading buffer before analysis by SDS-PAGE on 10 % Bis-Tris gels. Identity of STII enterotoxin was confirmed by mass spectrometry (PNAC, University of Cambridge).

Minimum inhibitory concentration (MIC) determinations

C43 (DE3) Δ*acrAB* Δ*macAB* bearing pETDuet MacAB wild type or variant were induced with 0.2 mM IPTG for 1 hour before addition to wells of a 96 well plates containing 0.2 mM IPTG, 100 µg/ml carbenicillin and 2-fold serial dilution of the indicated drug in LB medium (final volume 180 µl per well). Dilutions were from a 1024 µg/ml stock for ethidium bromide, chlorhexidine, SDS, gentamycin, tetracycline, ciprofloxacin, kanamycin, colistin, erythromycin, 8192 µg/ml for bacitracin and 512 µg/ml for chloramphenicol. For disulfide crosslinking experiments, 0.2mM $CuCl_2$ or 2mM DTT were added as indicated. MICs were assessed after 16 hours growth at 30 ºC. Experiments were repeated at least 3 times.

Purification of full-length *A. actinomycetemcomitans* MacB

E. coli C43 (DE3) transformed with pET28-*Aa*MacB was grown in 2YT medium at 30 °C. At OD_{600} 0.5, the temperature was reduced to 18 °C and protein expression induced by addition of 0.4 mM IPTG. After 16 hours further growth, cells were harvested by centrifugation (6000 *g*) and the cell pellets resuspended in 50 mM HEPES pH 7.5, 200 mM NaCl supplemented with protease inhibitor cocktail (Roche) and broken by 2 passages through a Constant Systems cell disruptor at 30000 psi. Unbroken cells and debris were removed by centrifugation (10 mins, 18000 g) before membranes were collected by centrifugation at 150000 *g* for 1 hour at 4 °C. Membranes were resuspended in 25 mM HEPES pH 7.5, 150 mM NaCl, 10 % (v/v) glycerol supplemented with protease inhibitors and solubilised by addition of lauryl maltose neopentyl glycol (LMNG; 1 % (w/v) final concentration). Insoluble material was removed by centrifugation (45 mins, 150000 *g*) and the solubilised membranes added to IMAC resin (Biorad Profinity). The resin was washed with 25 mM HEPES pH 7.5, 500 mM NaCl, 0.03 % LMNG, 10 mM imidazole and eluted with 25 mM HEPES pH 7.5, 500 mM NaCl, 0.03 % LMNG, 250 mM imidazole. Protein was buffer exchanged into 25 mM HEPES pH 7.5, 150 mM NaCl, 0.02 % LMNG and concentrated using Amicon Ultra 15 centrifugal concentrators (100 kDa cut-off). Selenomethionine incorporated *Aa*MacB was produced using a metabolic inhibition protocol (16). C43 (DE3) cells bearing pET28-*Aa*MacB plasmid were grown at 37 °C to OD_{600} 0.5 in M9 minimal media supplemented with 50 µg/mL kanamycin, 0.2 % (w/v) glucose, 2 mM $MgSO_4$, 0.1 mM $CaCl_2$ and 0.001 % (w/v) thiamine. 100 mg/L of threonine, lysine and phenylalanine, 50 mg/L of leucine, isoleucine and valine and 60 mg/L of selenomethionine were added and cells grown for a further 45 minutes. Protein expression was induced with 0.5 mM IPTG and the cells grown for a further 16h at 18 °C. Selenomethionine labelled protein was purified as native with the addition of 1 mM TCEP to all buffers. Incorporation of selenomethionine residues was confirmed by mass-spectrometry.

Purification of MacB periplasmic and cytoplasmic domains

E. coli C43 (DE3) cultures bearing pMacB-NBD or pMacB-Peri were grown at 37 °C on 2YT media supplemented with 50 μg/mL carbenicillin. Protein expression was induced with 1 mM IPTG at an OD_{600} ~0.6 and the temperature reduced to 18 °C. After 16 hours further growth, cells were harvested by centrifugation and the pellets frozen at -80 °C. Thawed cell pellets were resuspended in IMAC wash buffer (50 mM HEPES pH 7.5, 300 mM NaCl, 25 mM imidazole), and lysed by passage through a Constant Systems Cell Disruptor (30200 psi). Lysate was centrifuged at 30000 *g* for 30 min at 6 °C to remove cellular debris and the supernatant loaded onto an immobilised Ni-affinity column pre-equilibrated with the wash buffer (25 mM HEPES pH 7.5, 300 mM NaCl, 25 mM imidazole). Bound proteins were washed with 15 column volumes of wash buffer before elution in 50 mM HEPES pH 7.5, 300 mM NaCl, 300 mM imidazole. Protein samples were exchanged into 20 mM HEPES pH 7.2, 150 mM NaCl and concentrated to ~10 mg/mL using a centrifugal filter (Amicon 10 kDa nominal molecular weight cut-off) and frozen in liquid nitrogen before storage at -80 °C.

Purification of *E. coli* LolC periplasmic domain

BL21 (DE3) cells bearing plasmid pET24-EcperLolC were grown in 1L of 2YT medium supplemented with 50 μg/mL of kanamycin at 30°C. When the culture had achieved OD_{600} of 0.8 the temperature was reduced to 18 °C and protein expression induced with 0.1 mM IPTG. After 16 h further growth, cells were harvested by centrifugation at 4000 *g* and the pellet resuspended in 50 mL of 50 mM HEPES pH 7.5, 300 mM NaCl supplemented with protease inhibitor cocktail (Roche), lysozyme and DNAse. Bacteria were lysed by cell disruption (Constant Systems) at 30200 psi before removal of bacteria debris by ultracentrifugation (40 mins, 115000 g at 5 °C). The supernatant was incubated with Ni-NTA agarose resin (Qiagen) for 1h, washed with 20 mL of 20 mM HEPES pH 7.5, 300 mM NaCl, 20 mM imidazole and bound protein eluted with 10 mL of the same buffer supplemented with 250 mM imidazole. Eluted protein was exchanged into 20 mM HEPES pH 7.5, 150 mM NaCl using a 10 kDa cut-off centricon device (Amicon) and concentrated to 30 mg/mL, before flash freezing and storage at -80°C.

Crystallisation of full-length *A. actinomycetemcomitans* MacB, *E. coli* MacB periplasmic and cytoplasmic domains and *E. coli* LolC periplasmic domain

All crystallisation trials were conducted using the sitting drop vapour diffusion method in 2-drop MRC plates. Crystallisation drops were 1 μL in volume, composed of either 333 nL protein solution and 666 nL crystallisation reagent, or else 333 nL reagent and 666 nL protein, and were equilibrated over an 80 μL volume of the reagent alone. For *A. actinomycetemcomitans* MacB, protein aliquots (8 mg/mL) were thawed on ice and 5 mM MgATP or MgATPγS added immediately prior to crystallisation. Diffracting crystals were obtained in 100 mM Na-citrate pH 5.5, 21 % (v/v) PEG400 after 5 days and were harvested a few days later. Crystals of the selenomethionine derivative were

obtained in the same conditions. For cryoprotection, single crystals were transferred into a solution composed of 75 % (v/v) of the crystallisation reagent from the well reservoir and supplemented with 25 % (v/v) ethylene glycol and flash frozen in litholoops. Crystals of the MacB cytoplasmic domain were obtained using 2.8 M sodium formate, 100 mM sodium acetate pH 4.6. Crystals of the MacB periplasmic domain were first obtained as dense, non-diffracting needle clusters in 200 mM ammonium acetate, 30 % (v/v) glycerol ethoxylate, 100 mM MES pH 6.5. Subsequent streak seeding into a simple optimisation screen yielded thin near 2-dimensional plates in 35 % (v/v) glycerol ethoxylate, 100 mM sodium citrate pH 5.6. Further matrix-seeding into several different broad screens using these partially-optimised crushed-crystals yielded numerous conditions under which crystals grew. Data were collected from crystals grown from seeds in 30 % (v/v) pentaerythritol ethoxylate (15/4 EO/OH), 6 % (w/v) polyvinylpyrrolidone, 100 mM HEPES pH 7.5. For cryoprotection, single crystals were transferred into a solution composed of 75 % (v/v) of the crystallisation reagent from the well reservoir and 25 % (v/v) ethylene glycol before being flash frozen in litholoops. Crystallisation of the periplasmic domain of *E. coli* LolC was carried out by mixing 0.5 μL of protein at 10 mg/mL and 0.5 μL of reservoir solution composed of 0.2 M ammonium sulfate, 0.1 M sodium acetate at pH 4.6, 30% (w/v) of PEG 2000 MME. Crystals were grown at 15 °C by the sitting drop vapour diffusion method over a reservoir of 80 μL in MRC plates. The cryoprotection solution was composed of the reservoir solution supplemented with 25% (v/v) of glycerol before being flash frozen in nylon loops.

Structure determination – *E. coli* MacB periplasmic and cytoplasmic domains

X-ray data was collected at Diamond Light Source (UK) and structure solution used programmes from the CCP4 suite (17). Data were integrated with Imosflm (18), scaled with Aimless (19), and phased by molecular replacement using Phaser (20). The *E. coli* periplasmic domain was phased using a search model comprising the separated subdomains of the *A. actinomycetemcomitans* periplasmic domain (21) (PDB code 3FTJ). For the cytoplasmic domain, molecular replacement used the nucleotide binding domain (NBD) from MJ0796 (22) (PDB code 1L2T) as a search probe. To minimise phase bias, new phases were calculated using density modification implemented in Parrot (23) without recombination with the starting phases. Structural models were built with Buccaneer (24) using the density modified map as a starting point followed by cycles of model building and refinement using Coot (25) and Refmac (26). Non-crystallographic symmetry (NCS) restraints were used throughout refinement where possible. Validation was assisted with tools from Coot (25), Procheck (27), Rampage (28), and Molprobity (29). For the MacB cytoplasmic domain, two crystal forms were obtained – the first in space group $C222_1$ and another in space group $P6_122$. Statistics for crystallographic datasets and refined models pertaining to the MacB soluble domain structures are presented in **Table S2**. Coordinates and structure factors have been deposited with the protein

databank, accession codes **5LJA** (cytoplasmic form I), **5LJ9** (cytoplasmic form II) and **5LJ8** (periplasmic domain).

Structure determination – full-length *A. actinomycetemcomitans* MacB

Two datasets were collected at Soleil Proxima2 from a single crystal at distinct locations with a starting phi rotation 90° apart. A further dataset was collected at Diamond I24 on a second crystal isomorphous to the first. Each dataset was integrated and scaled using Imosflm (18) and Aimless (19). Radiation damage in each dataset was judged from the batch behaviour of overall statistics such as I/σ(I) and R_{merge} in the high-resolution bin. Data taken from the first part of each of all three datasets was merged and scaled using Aimless (19), and a high resolution cut-off chosen (3.35 Å) taking into account the I/σ(I), completeness and $CC_{½}$ in the outer resolution bin. Similar considerations were made for the $P6_522$ dataset.

The location of the cytoplasmic domain within the $P2_1$ cell was determined using molecular replacement with Phaser (20). A two-copy solution was found in space group $P2_1$ using the *E. coli* MacB cytoplasmic domain. After remodelling the *A. actinomycetemcomitans* sequence on the molecular replacement probe, further density was apparent in the asymmetric unit but was not easily interpreted. Searching the hexagonal data using the partially refined dimer from the $P2_1$ solution yielded a clear solution in space group $P6_522$ with a single molecule located beside the two-fold crystal symmetry axis. Inspection of the $P6_522$ density map revealed tubular density corresponding to the 4 transmembrane helices. The helices were modelled in Coot (25) as geometrically perfect polyalanine α-helices and this model transferred back to the $P2_1$ form. After a round of refinement with Refmac (26) (including jelly-body and NCS restraints), density modification protocols were employed with Parrot (23), DM and Resolve (30). The density-modified maps clarified the connectivity and directions of the transmembrane helices allowing these to be rebuilt and refined. Subsequent molecular replacement searches using the Sabre subdomain from the *A. actinomycetemcomitans* MacB periplasmic domain as a probe (keeping the cytoplasmic domain and polyalanine TM helices fixed) revealed the location of the Sabre subdomains. After phase calculation, the missing Porter domain was identified by manual inspection of the map. The Porter subdomains were manually placed in Coot (25) and refined using rigid body protocol in Refmac (26). Phases calculated during subsequent NCS-restrained maximum likelihood refinement of this model were used as a starting point for modification in Resolve (30) giving a map for use in model building. Once the majority of the protein main chain was built and the connectivity established, the $P2_1$-form polyalanine model was used to back-solve the $P6_522$ native and selenomethionine datasets by molecular replacement. Calculation of an anomalous scattering map using the selenomethionine dataset revealed locations of the Selenium positions informing the location of the methionines in the MacB polyalanine model. Returning to the $P2_1$ dataset, the model was updated with the methionine positions and

sequence assignments made where possible. Cycles of model building and maximum likelihood refinement were used to iteratively improve the model including additions of side chains. Non-crystallographic symmetry restraints were applied throughout. Inspection of the NBD revealed density for ATPγS, which was modelled as ATP and manually placed with assistance from real space fitting procedures in Coot (25). It was not possible to unambiguously identify the location of the oxygen-replacing sulfur in the ATPγS molecule. Near the end of refinement, validation tools from Coot (25), Molprobity (29), and Rampage (28) were used to guide further improvement of the model. In the final stages, refinement was switched from Refmac (26) to phenix.refine (31, 32). More than 120 iterative rounds of modelling and refinement were used to complete the model of MacB in space group $P2_1$. The final model of the $P2_1$ crystal form includes two MacB monomers, two ATP molecules, two magnesium ions and 4 crystallographically ordered waters. Residues 240-245, 312-324, 437-444 were not sufficiently well-resolved to model.

The structure of the $P6_522$ MacB crystal form was solved using the 3.35 Å structure of the $P2_1$ form as a starting model. Since the location of the NBD in the $P6_522$ cell was already known, a single monomer of the $P2_1$-form MacB structure was superposed using SSM (33) and subjected to rigid body refinement against the $P6_522$ data. This served as an initial model for the $P6_522$ form, which was then further improved by multiple iterations of model editing with Coot (25) and refinement with phenix.refine (31) using the $P2_1$ structure as a reference model. As refinement neared convergence, reference model restraints were released giving improvements in both R_{work} and R_{free}. Validation used tools from Coot (25), Procheck (27) and Rampage (28).

A final MacB structure was solved at 3.25 Å by refining the $P2_1$ form against data collected from a single crystal that was co-crystallised with regular ATP. No significant differences were observed, but the most complete model was derived from the 3.35 Å data. PDB accession codes for the full-length *A. actinomycetemcomitans* MacB are **5LIL** and **5LJ7** for the 3.35 Å and 3.25 Å monoclinic ($P2_1$) form and **5LJ6** for the hexagonal ($P6_522$) form.

Analysis of protein structures were assisted by various programs; the Dali server (34) was used for comparison with known structures, SSM superpose (33) for structural superpositions, ClustalOmega (35) for multiple sequence alignments. Positioning of MacB within the lipid bilayer was predicted using MEMEMBED (36). Analysis and visualisation of cavities within proteins was performed with POREWALKER (9) and HOLLOW (8). The homology model of *E. coli* MacB in the ATP bound state was constructed in I-TASSER (37) based on the full length *A. actinomycetemcomitans* MacB with assistance from our structures of the *E. coli* NBD (**5LJA**, **5LJ9** and periplasmic domains (**5LJ8)**. Structure images and movies were produced with PyMOL (38).

Structure determination – *E. coli* LolC periplasmic domain

Data were collected under cryogenic conditions at beamline I03 at Diamond Light Source (UK). The structure was refined with the CCP4 package (17). Images were integrated with Imosflm (18) and scaled with Aimless (19). The structure was solved by molecular replacement with Phaser (20) using the periplasmic domain of *A. actinomycetemcomitans* MacB (PDB 5LIL) as search model, but conserving only the β-sheet of the Porter subdomain. Electron density was improved with Parrot (23) before building the model with Buccaneer (24) and several rounds of manual refinement using Coot (25) and Refmac (26) with NCS restraints. Data collection and refinement statistics are shown in **Table S7.**

Supplementary References

1. Hollenstein K, Frei DC, Locher KP (2007) Structure of an ABC transporter in complex with its binding protein. *Nature* 446(7132):213–216.
2. Korkhov VM, Mireku SA., Locher KP (2012) Structure of AMP-PNP-bound vitamin B12 transporter BtuCD–F. *Nature* 490(7420):367–372.
3. Xu K, et al. (2013) Crystal structure of a folate energy-coupling factor transporter from *Lactobacillus brevis*. *Nature* 497(7448):268–71.
4. Dawson RJP, Locher KP (2006) Structure of a bacterial multidrug ABC transporter. *Nature* 443(7108):180–185.
5. Lee J-Y, et al. (2016) Crystal structure of the human sterol transporter ABCG5/ABCG8. *Nature*:1–17.
6. Luo Q, et al. (2017) Structural basis for lipopolysaccharide extraction by ABC transporter $LptB_2FG$. *Nat Struct Mol Biol* 24(5):469–474.
7. ter Beek J, Guskov A, Slotboom DJ (2014) Structural diversity of ABC transporters. *J Gen Physiol* 143(4):419–435.
8. Ho BK, Gruswitz F (2008) HOLLOW: generating accurate representations of channel and interior surfaces in molecular structures. *BMC Struct Biol* 8(1):49.
9. Pellegrini-Calace M, Maiwald T, Thornton JM (2009) PoreWalker: A novel tool for the identification and characterization of channels in transmembrane proteins from their three-dimensional structure. *PLoS Comput Biol* 5(7).
10. Krissinel E, Henrick K (2007) Inference of macromolecular assemblies from crystalline state. *J Mol Biol* 372(3):774–97.
11. Yamanaka H, Kobayashi H, Takahashi E, Okamoto K (2008) MacAB is involved in the secretion of *Escherichia coli* heat-stable enterotoxin II. *J Bacteriol* 190(23):7693–7698.
12. Viklund H, Elofsson A (2008) OCTOPUS: improving topology prediction by two-track ANN-based preference scores and an extended topological grammar. *Bioinformatics* 24(15):1662–1668.
13. Miroux B, Walker JE (1996) Over-production of Proteins in *Escherichia coli*: Mutant Hosts that Allow Synthesis of some Membrane Proteins and Globular Proteins at High Levels. *J Mol Biol* 260(3):289–298.
14. Datsenko KA, Wanner BL (2000) One-step inactivation of chromosomal genes in *Escherichia coli* K-12 using PCR products. *Proc Natl Acad Sci U S A* 97(12):6640–5.
15. Cherepanov PP, Wackernagel W (1995) Gene disruption in *Escherichia coli*: TcR and KmR cassettes with the option of Flp-catalyzed excision of the antibiotic-resistance determinant. *Gene* 158(1):9–14.

16. Van Duyne GD, Standaert RF, Karplus PA, Schreiber SL, Clardy J (1993) Atomic Structures of the Human Immunophilin FKBP-12 Complexes with FK506 and Rapamycin. *J Mol Biol* 229(1):105–124.
17. Winn MD, et al. (2011) Overview of the CCP4 suite and current developments. *Acta Crystallogr Sect D Biol Crystallogr* 67:235–242.
18. Battye TGG, Kontogiannis L, Johnson O, Powell HR, Leslie AGW (2011) iMOSFLM: A new graphical interface for diffraction-image processing with MOSFLM. *Acta Crystallogr Sect D Biol Crystallogr* 67:271–281.
19. Evans PR, Murshudov GN (2013) How good are my data and what is the resolution? *Acta Crystallogr Sect D Biol Crystallogr* 69(7):1204–1214.
20. McCoy AJ, et al. (2007) Phaser crystallographic software. *J Appl Crystallogr* 40:658–674.
21. Xu Y, et al. (2009) Crystal structure of the periplasmic region of MacB, a noncanonic ABC transporter. *Biochemistry* 48(23):5218–5225.
22. Smith PC, et al. (2002) ATP binding to the motor domain from an ABC transporter drives formation of a nucleotide sandwich dimer. *Mol Cell* 10(1):139–149.
23. Cowtan K (2010) Recent developments in classical density modification. *Acta Crystallogr Sect D Biol Crystallogr* 66:470–478.
24. Cowtan K (2006) The Buccaneer software for automated model building. 1. Tracing protein chains. *Acta Crystallogr Sect D Biol Crystallogr* 62:1002–1011.
25. Emsley P, Lohkamp B, Scott WG, Cowtan K (2010) Features and development of Coot. *Acta Crystallogr Sect D Biol Crystallogr* 66:486–501.
26. Murshudov GN, et al. (2011) REFMAC5 for the refinement of macromolecular crystal structures. *Acta Crystallogr Sect D Biol Crystallogr* 67:355–367.
27. Laskowski RA., MacArthur MW, Moss DS, Thornton JM (1993) PROCHECK: a program to check the stereochemical quality of protein structures. *J Appl Crystallogr* 26(2):283–291.
28. Lovell SC, et al. (2003) Structure validation by C alpha geometry: phi,psi and C beta deviation. *Proteins-Structure Funct Genet* 50(3):437–450.
29. Chen VB, et al. (2010) MolProbity: All-atom structure validation for macromolecular crystallography. *Acta Crystallogr Sect D Biol Crystallogr* 66:12–21.
30. Terwilliger TC (2003) research papers Statistical density modification using local pattern matching research papers. *Acta Crystallogr Sect D*:1688–1701.
31. Afonine P V., et al. (2012) Towards automated crystallographic structure refinement with phenix.refine. *Acta Crystallogr Sect D Biol Crystallogr* 68(4):352–367.
32. Adams PD, et al. (2002) PHENIX: Building new software for automated crystallographic structure determination. *Acta Crystallogr Sect D Biol Crystallogr* 58(11):1948–1954.
33. Krissinel E, Henrick K (2004) Secondary-structure matching (SSM), a new tool for fast protein structure alignment in three dimensions. *Acta Crystallogr Sect D Biol Crystallogr* 60(12

I):2256–2268.

34. Holm L, Rosenström P (2010) Dali server: Conservation mapping in 3D. *Nucleic Acids Res* 38(2):545–549.
35. Sievers F, et al. (2011) Fast, scalable generation of high-quality protein multiple sequence alignments using Clustal Omega. *Mol Syst Biol* 7(1):539.
36. Nugent T, Jones DT (2013) Membrane protein orientation and refinement using a knowledge-based statistical potential. *BMC Bioinformatics* 14(1):276.
37. Yang J, et al. (2014) The I-TASSER Suite: protein structure and function prediction. *Nat Methods* 12(1):7–8.
38. DeLano WL (2002) The PyMOL Molecular Graphics System. *Schrödinger LLC* http://www.pymol.org